ORIGINAL ARTICLE

Antonios Monokrousos · Luca Brandt · Catherine Mavriplis ·
Dan S. Henningson

Optimal disturbances above and upstream of a flat plate with an elliptic-type leading edge

Abstract Adjoint-based iterative methods are employed to compute linear optimal disturbances in a spatially growing boundary layer around an elliptic leading edge. The Lagrangian approach is used where an objective function is chosen and constraints are assigned. The optimisation problem is solved using power iterations combined with a matrix-free formulation, where the state is marched forward in time with a standard direct numerical simulation solver and backward with the adjoint solver until a chosen convergence criterion is fulfilled. We consider the global and, more relevant to receptivity studies, the upstream localised optimal initial condition leading to the largest possible energy amplification at time T. We find that the two-dimensional initial condition with the largest potential for growth is a Tollmien–Schlichting-like wave packet that includes the Orr mechanism and is located inside the boundary layer downstream of the leading edge. Three-dimensional optimal disturbances induce streaks by the lift-up mechanism. Requiring the optimal initial condition to be localised upstream of the plate enables us to better study the effects of the leading edge on the boundary layer receptivity mechanisms. Two-dimensional upstream disturbances are inefficient at triggering unstable eigenmodes, whereas three-dimensional disturbances induce streamwise streaks with significant growth.

Keywords Boundary layer instabilities · Receptivity · Adjoint-based optimisation · Nonmodal growth

1 Introduction

The flat plate boundary layer has been a test bed for various approaches when studying hydrodynamic stability. Although a fairly simple flow configuration, the relevance of this flow type arises from the fact that it features many aspects of external flows, thus being an adequate model of these flows. In stability studies, further simplifications of the flat plate boundary layer are often introduced, e.g. the assumption of a locally parallel flow with a Fourier decomposition in the streamwise direction [9,23] or of a slowly varying flow amenable to parabolised equations [2,15,17,27]. Two- and three-dimensional disturbances have been studied using global modes, providing an accurate representation of the stability of the streamwise growing boundary layer [1].

Leading edge effects are far less studied. Goldstein et al. [12] and Goldstein and Wundrow [13] consider through asymptotic analysis flow around a flat plate of finite thickness with an upstream vortical free-stream disturbance. Since the 1990s, there are also a small number of numerical simulations of flow around leading

---

A. Monokrousos · L. Brandt (✉) · D. S. Henningson
SeRC, Linné Flow Centre, KTH Mechanics, 100 44 Stockholm, Sweden
E-mail: luca@mech.kth.se

C. Mavriplis
Department of Mechanical Engineering, University of Ottawa, Ottawa, Canada

edges with different geometry, mainly dealing with acoustic receptivity (see [16,31] and the review by Saric et al. [24] for early studies). These studies considered the evolution of well-defined disturbances that are investigated individually, whereas we present here an optimisation aiming to identify the most dangerous external disturbances.

Recently, the development of the time-stepper technique made it possible to tackle more complicated flow configurations with two- and three-dimensional disturbances. This technique enables stability studies for any flow type and geometry, for which a direct numerical simulation (DNS) is feasible. The only requirement is a numerical solver of the time-dependent linearised Navier–Stokes equations and the corresponding adjoint equations. This approach was adopted by Tuckerman and Barkley [29] and later by Barkley et al. [4], Blackburn et al. [5] and Theofilis [28], for example.

The present study is an extension of previous work by Monokrousos et al. [20] where optimal disturbances were computed for a flat plate boundary layer. Here, we take a step further and include the plate leading edge while retaining a fairly high Reynolds number where transitional or even turbulent flow is typically observed. In particular, we focus on the effect of the leading edge and investigate how it changes the optimal disturbances and how the boundary layer is optimally excited by oncoming perturbations. In recent studies [25,26], we have considered the linear and nonlinear receptivity to free-stream vorticity of the flow past a flat plate with an elliptic leading edge. In those works, disturbances periodic in time and space are considered and the relevance of the three vorticity components of natural free-stream turbulence is investigated by considering axial, vertical and spanwise vorticity separately for different angular frequencies. No optimisation of the external disturbance was attempted as done here where the most dangerous linear disturbance component is determined as part of the results. Nonlinear optimisation has been performed for the simpler Couette flow in [21]. Further, we consider here an initial value problem and not a forced problem as in Schrader et al. [25] and Brandt et al. [7] for the case of an infinitely thin plate.

The flow case, for the chosen parameters, is classified as a 'noise amplifier' (rather than an 'oscillator'), characterised by convective instabilities when studied in the local framework. From the global point of view, the flow is asymptotically stable to linear disturbances. Therefore, it is more adequate to study the transient growth problem in the context of non-modal analysis.

2 Optimisation problem

We solve the linearised incompressible Navier-Stokes equations

$$\partial_t \mathbf{u} + (\mathbf{U} \cdot \nabla)\,\mathbf{u} + (\mathbf{u} \cdot \nabla)\,\mathbf{U} = -\nabla p + Re^{-1}\Delta\mathbf{u}, \tag{1}$$
$$\nabla \cdot \mathbf{u} = 0,$$

where $\mathbf{u}$ is the disturbance velocity and $\mathbf{U}$ the baseflow velocity, p denotes the pressure and Re is the Reynolds number (defined in Sect. 3.2). The symbol ∂_t stands for the partial derivative with respect to time, and $\nabla = (\partial/\partial x, \partial/\partial y, \partial/\partial z)$ is the nabla operator, with x, y and z being the streamwise, vertical and spanwise coordinates. To determine the optimal disturbances at and upstream of the leading edge, the Lagrangian approach is used where an objective function is chosen and constraints are assigned. The method is equivalent to finding the leading eigenpair of the composite direct-adjoint Navier–Stokes evolution operator [3]. For a demonstration in a more general framework, the reader is refereed to Mao et al. [19]. Our objective function is the integral in space of the disturbance kinetic energy at some final time T,

$$\mathcal{J}(\mathbf{u}) = (\mathbf{u}(T), \mathbf{u}(T)). \tag{2}$$

The constraints chosen are the demand for $\mathbf{u}$ to satisfy the linearised Navies-Stokes equations and the requirement for the initial condition to be divergence free and of unit energy norm inside the domain Λ (being zero outside Λ). Hence, the Lagrangian functional is written as

$$\mathcal{L}(\mathbf{u}, \mathbf{v}, \gamma, \psi) = (\mathbf{u}(T), \mathbf{u}(T)) - \int_0^T (\mathbf{v}, (\partial_t - \mathcal{A})\,\mathbf{u})\,\mathrm{d}\tau$$
$$- \gamma\left((\mathbf{u}(0), \mathbf{u}(0))_\Lambda - 1\right) - (\psi, \nabla \cdot \mathbf{u}(0))_\Lambda \tag{3}$$

where $\mathbf{v}$, γ and ψ are the Lagrange multipliers, $\mathcal{A}$ indicates the governing linear operator and the inner product, defined by $(\cdot, \cdot)_\Lambda$, corresponds to an integral over Λ. We seek to determine $\mathbf{u}$, $\mathbf{u}(0)$, $\mathbf{u}(T)$, $\mathbf{v}$, γ and ψ such that $\mathcal{L}$ is stationary, a necessary condition for first order optimality. This is achieved by requiring that the variation of $\mathcal{L}$ be zero, leading to a set of conditions to be fulfilled simultaneously: the solution must satisfy the governing equations,

$$(\partial_t - \mathcal{A})\mathbf{u} = 0, \tag{4}$$

with the normalisation condition

$$(\mathbf{u}(0), \mathbf{u}(0))_\Lambda = 1. \tag{5}$$

Further, the adjoint system, integrated backward in time, must be fulfilled,

$$(-\partial_t - \mathcal{A}^\dagger)\mathbf{v} = 0, \tag{6}$$

where $\mathcal{A}^\dagger$ is the adjoint Navier–Stokes operator, and the initial and optimality conditions are

$$\begin{aligned} \mathbf{v}(T) &= \mathbf{u}(T), \\ \mathbf{u}(0) &= \gamma^{-1}(\mathbf{v}(0) - \nabla\psi)|_\Lambda. \end{aligned} \tag{7}$$

In the above, the scalar field ψ represents a projection to a divergence-free space, where the pressure-like scalar field ψ is solution to a Poisson equation. More details are provided in [20] for a generic three-dimensional disturbance while here the method is applied to disturbances initially localised only in two-dimensions, i.e. the localisation is applied to a single spanwise Fourier mode. Note also that the projection of the initial condition onto the divergence-free space is performed by a GMRES iterative algorithm before marching in time the forward problem [11].

To solve the optimisation problem, a matrix-free method is employed, where the state is marched forward in time with a standard DNS solver and backward in time with the corresponding adjoint solver until a chosen convergence criterion is fulfilled. The initial and normalisation conditions for the two systems are given by (7). With this approach, we propose a systematic and direct method to compute the receptivity of the boundary layer to external disturbances. In this framework, the computed optimal modes can be used as a projection basis to quantify the ability of oncoming free-stream disturbances to initiate perturbations in the boundary layer.

3 Numerical approach

3.1 Numerical code

The governing equations are solved with the spectral element code Nek5000 developed by Fischer [30]. The equations are discretised by a weighted residual spectral element method (see Patera [22]), using a multi-domain decomposition while preserving high order accuracy. Inside each sub-domain (referred to as spectral element), the fields are represented by a spectral decomposition using Legendre polynomial Lagrangian interpolants, where the grid points are allocated according to a Gauss–Lobatto Legendre distribution (see Fischer et al. [11], for details). The numerical method for the computation of the optimal initial condition is validated against previous results from Monokrousos et al. [20] obtained by a global spectral method (described in [10]).

3.2 Flow case

We consider the flow around a flat plate with an elliptic leading edge. The leading edge features the shape of a modified super ellipse,

$$\left(\frac{y}{b}\right)^2 = 1 - \left(\frac{a-x}{a}\right)^p, \qquad p = 2 + \left(\frac{x}{a}\right)^2, \tag{8}$$

with zero curvature at the juncture to the flat section so that no disturbances are introduced at the junction, i.e. the plate does not scatter disturbances at its leading edge. The ratio a/b defines the leading edge bluntness, chosen here to be 6. This results in a relatively blunt shape. The Reynolds number of the flow is $Re = bU/\nu$ based on the half thickness of the plate (b), the free-stream velocity (U) and the kinematic viscosity of the fluid (ν). We only consider half of the body and impose a symmetry condition along the stagnation streamline

Table 1 Spatial resolution of the two- and three-dimensional computational domains for flow over a flat plate with an elliptic leading edge of aspect ratio 6, where n_t, n_n and n_z denote the number of spectral elements used along the surface-tangential, surface-normal and spanwise directions, and n_{tot} is the total amount of elements

Case	n_t	n_n	n_z	n_{tot}	N	$n_{v,tot}$	$n_{p,tot}$	Re_x
2D low Re	100	17	–	1,700	9	138,754	108,800	1e5
2D high Re	160	19	–	3,040	9	246,411	194,560	6e5
2D high Re-L	219	21	–	4,599	9	374,680	294,336	9e5
3D	124	19	3	7,068	9	5,379,472	3,618,816	3e5

N is the spectral order, defining the number of polynomials used to approximate the flow solution on the elements. $n_{v,tot} = (n_t N + 1)(n_n N + 1)(n_z N + 1)$ is the number of nodes of the velocity grid and $n_{p,tot} = n_t n_n n_z (N - 1)^3$ the nodes of the pressure grid. Re_x denotes the outflow Reynolds number

ahead of the leading edge. Most of the results presented are obtained for a Reynolds number of $Re = 3000$. We also include a few results for a lower Reynolds number, $Re = 1000$. The streamwise Reynolds number $Re_x = xU/\nu$ will occasionally be used when presenting the results, where x is the distance from the leading edge. We refer to the study by Schrader et al. [25] for a validation of the steady base flow around the leading edge against numerical and experimental results published in the literature.

3.3 Resolution

Table 1 compiles the parameters (number of elements and spectral order) defining the spatial discretisation of the computational domain. The total number of elements depends on the length of the domain, where the two-dimensional simulations are carried out on a longer domain than the three-dimensional simulations in order to fully capture the unstable region of the two-dimensional Tollmien–Schlichting (TS) waves. In all simulations, the elements are clustered near the wall and in the leading edge vicinity.

4 Results

We investigate the disturbances causing the largest transient energy growth for different optimisation times. Since the base flow is homogeneous in the spanwise direction, disturbances of different spanwise periodicity can be studied separately. Owing to the significant computational cost of the iterative optimisation procedure, we are forced to restrict the study to a few typical cases reflecting the essential physical mechanisms.

4.1 Two-dimensional optimal initial conditions

4.1.1 Global optimal initial conditions

Two-dimensional optimal disturbances are computed for two different Reynolds numbers, $Re = 1000$ and 3000. Here, we drop the constraint of localising the optimal disturbance structure upstream of the leading edge (last term in Eq. 3).

In Fig. 1, the disturbance energy $E(t)/E_0$ is shown for various optimisation times. $E(t)$ is defined as

$$E(t) = (\mathbf{u}(t), \mathbf{u}(t)),   \tag{9}$$

and E_0 denotes the initial energy (time $t = 0$). The red line in Fig. 1 is the energy envelope. Figure 1a shows results for the low Reynolds number ($Re = 1000$) where the boundary layer is locally stable everywhere. The outflow Reynolds number based on the distance to the leading edge is $Re_x = 10^5$. In this case, the only possibility of energy growth is through the Orr mechanism.

Figure 1b reports results for the higher Reynolds number ($Re = 3000$). In this case, we observe that locally unstable TS wave packets are generated and amplify exponentially as they are convected downstream. The maximum time for energy growth is here governed by the downstream extension of the computational box, i.e. a longer box would enable longer optimisation times and more space for the exponential instability to grow. Additionally, we note a local maximum for short optimisation times which corresponds again to a pure Orr mechanism, being active on small time scales. The energy decay seen for large optimisation times is due to the
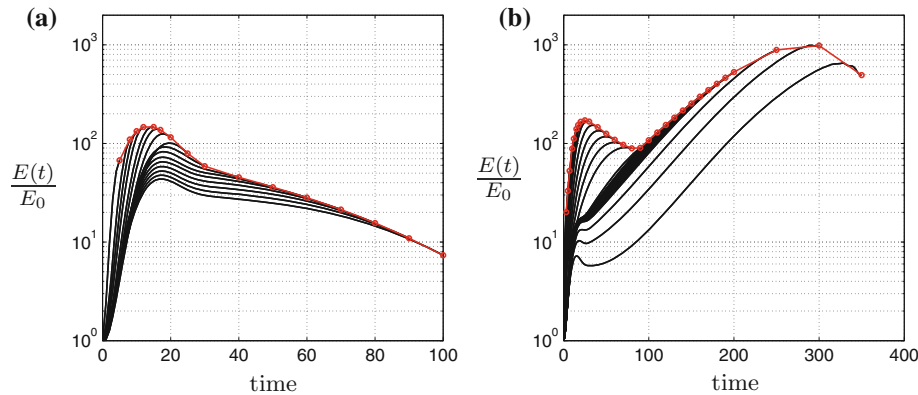
Fig. 1 Disturbance energy $E(t)/E_0$ versus optimisation times for two-dimensional disturbances at **a** $Re = 1000$ and **b** $Re = 3000$
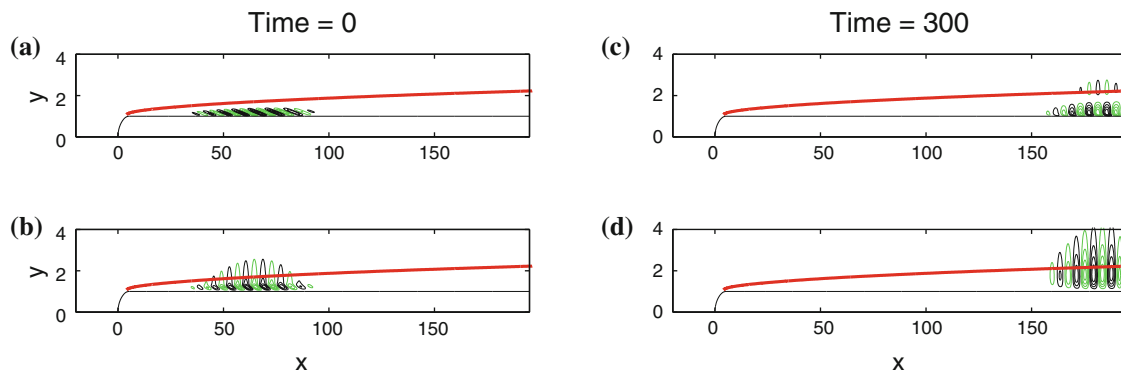

Fig. 2 Spatial structure of optimal initial condition and corresponding response at $Re = 3000$. Initial condition: **a** streamwise component, **b** wall-normal component. Response: **c** streamwise component, **d** wall-normal component. The *red line* indicates the boundary layer edge, δ_{99} (colour figure online)

fact that these disturbances gradually exit our computational domain and thus their spatially integrated energy decays.

In Fig. 2a,b, the spatial structure of the optimal disturbance is shown for the optimal time $T = 300$ and a Reynolds number of $Re = 3000$. The flow structures clearly display the Orr mechanism generating an unstable wave packet (Fig. 2c,d; see also references [1,20]).

4.1.2 Localised two-dimensional optimal initial conditions

We study two-dimensional optimal initial conditions that are localised in space. The aim is to investigate how an upstream disturbance optimally penetrates the boundary layer around the curved leading edge and subsequently generates a perturbation that can undergo streamwise growth inside the boundary layer. Indeed, two-dimensional TS waves are the driver of boundary layer transition to turbulence in flight condition where we typically have low levels of free-stream turbulence ($<0.4\%$) as well as in wind tunnels of good quality and reduced noise.

Figure 3 displays the localised initial condition upstream of the leading edge and the flow at the optimisation time $T = 700$: here, we can see the reduction of the disturbance wavelength when interacting with the boundary layer and the formation of a weak TS wave packet. For initial perturbations limited to a sub-domain upstream from the leading edge, the results obtained are largely in line with those reported in the literature. The upstream localised vortical disturbances turn out to be rather inefficient in penetrating the boundary layer. Furthermore, the disturbance generated inside the boundary layer is significantly damped during the initial phase and consists of a wave packet characterised by a relatively high streamwise wavenumber—larger than that of the locally unstable TS wave. It turns out that the optimisation procedure favours a less unstable wave packet over the most unstable waves since the former is probably more capable of penetrating the shear layer. The growth of
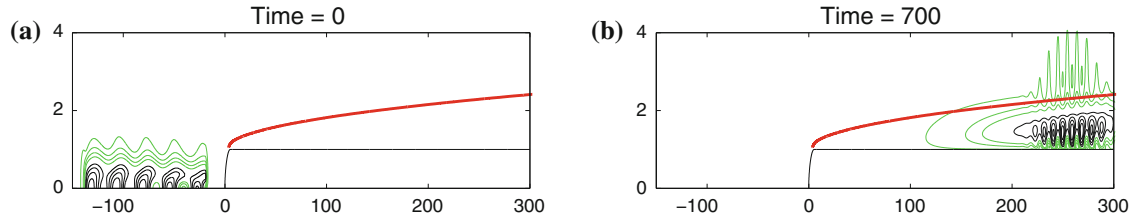
Fig. 3 Spatial structure of optimal localised initial condition and corresponding response at $Re = 3000$ and outflow $Re_x = 900000$. Streamwise velocity component of **a** the initial condition and **b** the optimal response. The *red line* indicates the boundary layer edge, δ_{99} (colour figure online)
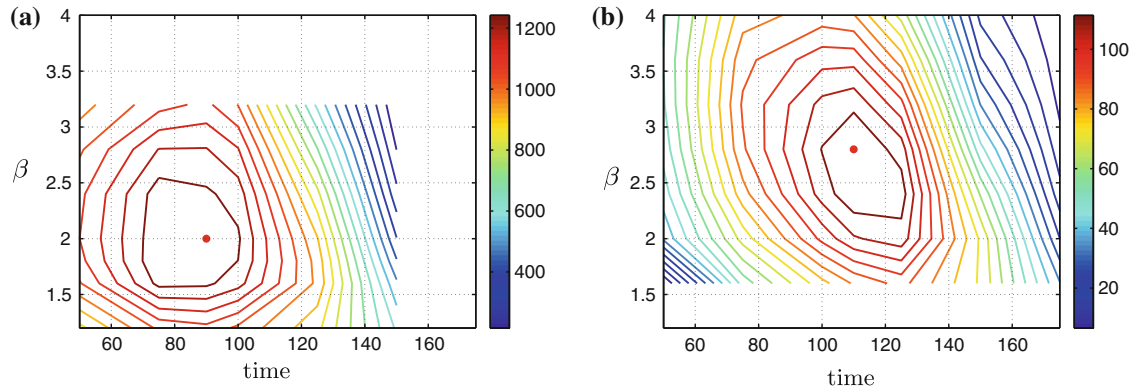

Fig. 4 Contour levels of energy gain $G = E(t)/E_0$ versus the final optimisation time and the spanwise wavenumber. **a** Non-localized and **b** localized initial disturbance condition. The Reynolds number is $Re = 3000$

the wave packet would be enhanced on an even longer computational domain with sufficient space for the TS waves to grow exponentially. Owing to the high computational cost of the iterative optimisation procedure, we were, however, forced to limit the length of the plate. This points to the limitations of the current approach for receptivity studies in the absence of a strong amplification mechanisms as in the case of the lift-up effect studied below.

Acoustic waves seem, therefore, the most efficient mean to trigger TS waves. Buter and Reed [8] have observed that vortical receptivity is lower than that to acoustic waves. For a significantly high frequency (F = 230), they have found that the coefficients for receptivity to vortical modes are about 1/3 than those for acoustic disturbances. In Schrader et al. [25], the values of the receptivity coefficients to spanwise free-stream vorticity are compared to those for acoustic receptivity from Wanderley and Corke [31] for a leading edge with aspect ratio equal to 20. The receptivity coefficients to vortical noise are lower by one order of magnitude than those to acoustic waves. In particular, the largest coefficient for vorticity is about 15 % of that for sound waves.

4.2 Three-dimensional optimal initial conditions

4.2.1 Global optimal initial conditions

When studying three-dimensional disturbances, we need to consider an additional parameter, namely the spanwise disturbance wavenumber β. Therefore, in order to determine the optimal value of β, we now loop over two parameters, the optimisation time and the spanwise wavenumber (two-dimensional parameter space).

In Fig. 4a, we plot iso-contours of the energy gain $G = E(t)/E_0$ for different optimisation times T and spanwise wavenumbers β. We identify a clear peak at $T = 90$ and $\beta = 2.0$. In order to understand the physical mechanisms behind this peak, we consider the spatial distribution of the disturbance velocities. The three velocity components of the optimal initial condition are shown in Fig. 5a, and the corresponding velocities of the response are depicted in Fig. 5b. We note a strong component-wise energy transfer, implying that the lift-up mechanism is active, where streamwise vortices induce streamwise streaks inside the boundary layer. For the present case, the initial energy content ($t = 0$) of the streamwise velocity component is only 6.3 % of the total energy, increasing to 91.3 % at the optimal time ($t = T$). The energy of the wall-normal (spanwise)
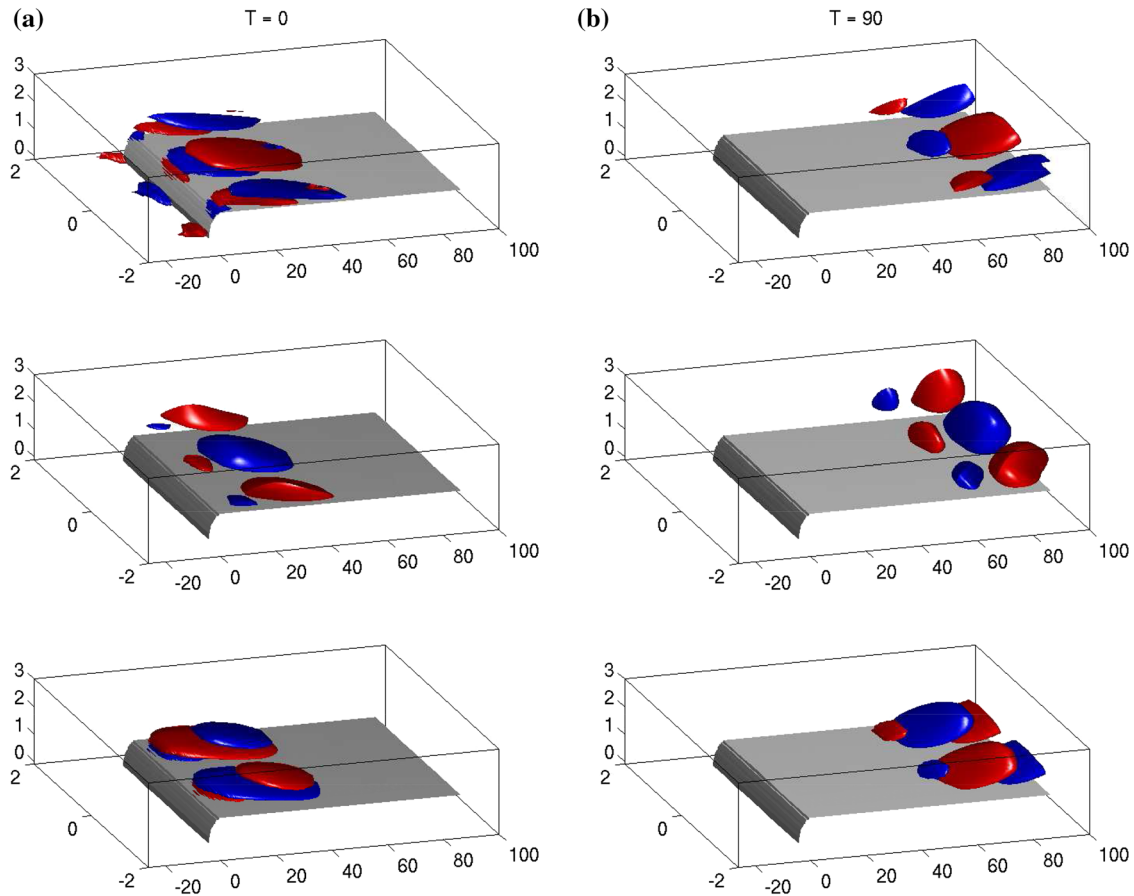
Fig. 5 a Optimal initial condition and **b** the corresponding flow response. Streamwise, wall-normal and spanwise velocities are shown from *top* to *bottom*. The energy growth is $G = 1.3 \times 10^3$ at a Reynolds number of $Re = 3000$. The Reynolds number at the outflow based on the distance from the leading edge is $Re_x = 300000$

velocity component decreases from 28.6 % (65.1 %) to 1.8 % (6.9 %) of the total disturbance energy. The total energy growth is $G = 1.3 \times 10^3$. Similar results were obtained by Andersson et al. [2] using the boundary layer equations and by Monokrousos et al. [20] in the global framework of a flat plate boundary layer without a leading edge. The emerging flow structures are plotted in Fig. 5b. We notice in Figure 5 that the Orr mechanism with the characteristic upstream leaning structures contributes partly to the downstream development of the disturbance.

For longer optimisation times, a rapid decay of the amplification is observed in Fig. 4 when disturbances leave our computational domain. As we increase the optimisation time, the optimal initial disturbance moves farther upstream so that the excited flow response stays inside the domain within the optimisation time. Beyond a certain value of T, the optimal initial condition moves upstream of the leading edge into a region without significant mean shear, which explains the lower amplification. In these cases, the initial disturbance resembles the localised optimal perturbation discussed in the next section. For short times T, on the other hand, the lift-up mechanism does not have enough time to fully exploit the shear in the boundary layer.

In order to compare our results with those from [20], where the wavenumber is scaled by the boundary layer displacement thickness, we need to re-scale the lengths and wavenumbers of our present formulation. In the units used in Ref. [20], the present optimal wavenumber is $\beta^* = 0.67$. This value is comparable to that in [20] ($\beta^* = 0.55$), where we ascribe the difference to the presence of the leading edge.

4.2.2 Optimal localised three-dimensional disturbances

As for the two-dimensional modes, we perform a parametric study to find the optimal time T and spanwise wavenumber β. In Fig. 4b, iso-contours of energy growth for different optimisation times and spanwise

wavenumbers are shown for the case of the upstream localised disturbance. The red dot corresponds to the maximum. The optimal disturbance occurs for $T = 125$ and $\beta = 2.8$. Comparing these values to those obtained for the global (non-localised) optimal, we identify two main differences: (i) the optimal time T is longer and (ii) the optimal spanwise wavenumber β is larger. The larger value of T is expected as the upstream localised perturbation needs additional time to travel to the leading edge and penetrate the boundary layer.

We have shown above that the receptivity to purely two-dimensional disturbances is very weak upstream of the leading edge. This observation can possibly explain why the optimal wavenumber β for the upstream localised case is larger than that of the global optimal: whereas larger values of β may, on the one hand, become less optimal with respect to the lift-up mechanism, the corresponding disturbances are, on the other hand, less damped when penetrating the shear layer at the leading edge. These two trends seem to be in balance at $\beta = 2.8$ ($\beta^* = 0.93$). The physical mechanisms pertaining to the energy growth appear to be similar in the cases of global and upstream localised optimal initial conditions. However, the Orr mechanism is absent in the latter case because there is no significant mean shear upstream of the leading edge, which could support an additional energy gain due to upstream leaning disturbance structures. As the streaks are the result of a robust amplification mechanism, the lift-up effect, the final disturbance is very similar when considering localised and non-localised optimal initial conditions [see e.g. 6,17]. However, the streamwise vortices creating those streaks appear to have a different wall-normal localisation: these vortices are lower and located inside the shear layer, closer to the wall, in the case of upstream localised disturbances, whereas they extend higher up when they are already above the flat plate at time zero.

The spatial distributions of the upstream localised optimal initial condition and the corresponding response are shown in Fig. 6a,b. As for the non-localised disturbance, most of the perturbation energy is initially in the cross-stream components (36.7 and 45.6 % in the normal and spanwise direction, respectively), whereas
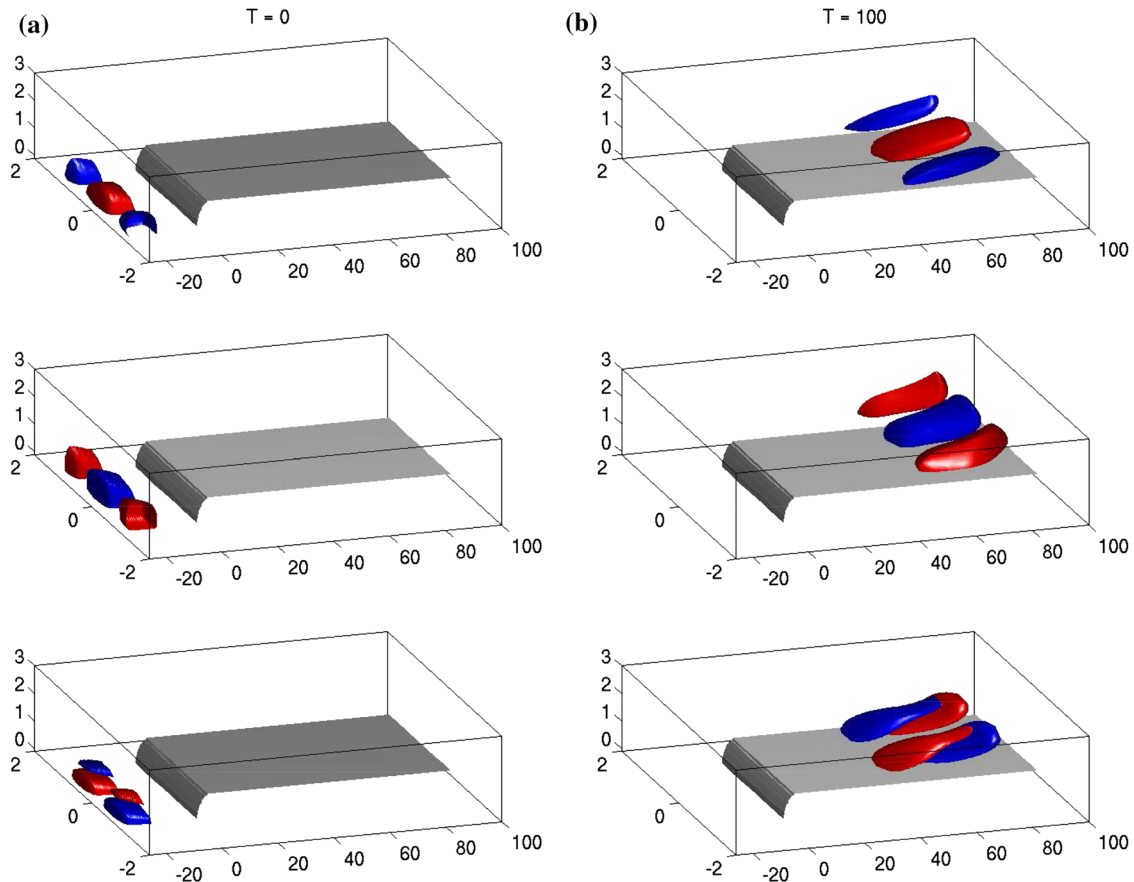

Fig. 6 a Localised optimal initial condition and **b** corresponding flow response. From *top* to *bottom*: streamwise, wall-normal and spanwise disturbance velocities. The energy growth is $G = 1.2 \times 10^2$ and the Reynolds number $Re = 3000$. The outflow Reynolds number (based on the distance from the leading edge) is $Re_x = 300000$

the streamwise velocity only carries 17.7 % of the total energy. At the final optimisation time, conversely, the streamwise component contains 93.6 % of the total energy, while the normal and spanwise components only account for 1.8 and 4.6 % of the disturbance energy, respectively. As long as the disturbance vortices travel upstream of the leading edge, they slowly decay similar to what is observed in decaying turbulence. However, once the vortices reach the region with strong mean shear near the stagnation point (after $T \approx 20$), they quickly start to transfer energy to the streamwise boundary layer streaks, extracting energy from the mean shear by the lift-up effect. It is thus important to include the leading edge effect in a receptivity study (see also [25]). The total energy growth is substantially weaker relative to the global (non-localised) optimals. This is attributed to the following reasons: (i) the Orr mechanisms cannot contribute to the energy gain upstream of the leading edge and (ii) the lift-up effect is active farther upstream relative to the non-localised case, where the local Reynolds number—and thus the transient growth potential—is lower (see [2]).

5 Conclusions

We have applied a Lagrange multiplier technique using the direct and adjoint linearised Navier–Stokes equations in order to quantify the disturbance growth potential in a flow over a flat plate with an elliptic leading edge at moderately high Reynolds numbers. We consider the optimal initial condition leading to the largest possible energy amplification at time T. In particular to understand the boundary layer response to external ambient noise, we compute an optimal disturbance localised upstream of the leading edge. This approach can be used to create a modal basis for a projection of free-stream disturbances, establishing a direct method for computing receptivity coefficients for externally excited flows. While this may not be the most efficient way to compute receptivity coefficients, it provides details about the most dangerous components of the incoming disturbances. The optimisation framework adopted is not restricted to streamwise slowly varying base flows, a common assumption of the first order approximation of the Orr–Sommerfeld–Squire formulation and the more advanced Parabolised Stability Equations approximation. Moreover, the method presented here allows us to include curved geometries and fully three-dimensional flow configurations.

We find that the two-dimensional initial condition with the largest potential for growth is a TS-like wave packet that includes the Orr mechanism in the initial growth phase and is located inside the boundary layer downstream of the leading edge. The growth of this optimal disturbance is linked to the exponentially unstable eigenmodes of the Blasius boundary layer, and it is limited by the streamwise extent of the computational box. The case of three-dimensional optimal disturbances exhibits a peak in the energy for a much earlier time (i.e. a more upstream location) and for a spanwise wavenumber of $\beta = 2.0$, relevant to the well-understood lift-up mechanism. This value is in close agreement with earlier studies of a similar nature [20].

The upstream localised optimal initial conditions are more interesting as they allow for a better understanding of the effects of the leading edge on the boundary layer receptivity. In this setting, the optimal disturbance conditions reside in the free stream upstream of the leading edge. We find that two-dimensional upstream disturbances are rather inefficient at triggering unstable wave packets. The flow around the leading edge has a strong damping effect on this type of disturbance, so that the optimisation procedure favours stable wave packets with lower damping in the initial boundary layer penetration phase over the downstream unstable (but initially highly damped) wave packets. Note that the present formulation does not allow acoustic waves to be admissible upstream disturbances, although they are probably the most effective in generating TS waves, see Haddad and Corke [14] and Wurz et al. [32] as examples of numerical studies where acoustic waves are imposed in an incompressible flow as oscillating harmonic free-stream boundary conditions. The present method can be extended to acoustic disturbances by considering sensitivity to and optimisation of boundary conditions, as done for example by Mao et al. [18,19] and in [7] for wall blowing and suction. Indeed, it is interesting to add that the approach suggested in [19] is also suitable to extend the present formulation to the spatial framework.

The three-dimensional, upstream localised disturbances turn out to be more efficient in perturbing the boundary layer than their two-dimensional counterparts. They are able to exploit the lift-up mechanism efficiently, although the local Reynolds number is lower than in the case of global optimal initial conditions (i.e. the streak generation happens farther upstream). Since the boundary layer streaks created by the upstream disturbance are located farther away from the wall than the TS waves of the two-dimensional scenario, they do not suffer from the high energy loss due to diffusion close to the wall. Additionally, the streamwise wavenumber

of the streaks is low and does not depend much on the (low) local Reynolds number, therefore rendering this instability mechanism robust.

References

1. Åkervik, E., Ehrenstein, U., Gallaire, F., Henningson, D.S.: Global two-dimensional stability measures of the flat plate boundary-layer flow. Eur. J. Mech. B/Fluids **27**, 501–513 (2008)
2. Andersson, P., Berggren, M., Henningson, D.S.: Optimal disturbances and bypass transition in boundary layers. Phys. Fluids **11**, 134–150 (1999)
3. Bagheri, S., Åkervik, E., Brandt, L., Henningson, D.S.: Matrix-free methods for the stability and control of boundary layers. AIAA J. **47**, 1057–1068 (2009)
4. Barkley, D., Blackburn, H.M., Sherwin, S.J.: Direct optimal growth analysis for timesteppers. Int. J. Numer. Meth. Fluids **57**, 1435–1458 (2008)
5. Blackburn, H.M., Barkley, D., Sherwin, S.J.: Convective instability and transient growth in flow over a backward-facing step. J. Fluid Mech. **608**, 271–304 (2008)
6. Brandt, L., Henningson, D.S.: Transition of streamwise streaks in zero-pressure-gradient boundary layers. J. Fluid Mech. **472**, 229–261 (2002)
7. Brandt, L., Pralits, J.O., Sipp, D., Marquet, O.: Effect of base flow variation on non-modal stability. J. Fluid Mech. **687**, 503–528 (2011)
8. Buter, T.A., Reed, H.L.: Boundary layer receptivity to free-stream vorticity. Phys. Fluids **6**(10), 3368–3379 (1994)
9. Butler, K.M., Farrell, B.F.: Three-dimensional optimal perturbations in viscous shear flow. Phys. Fluids A **4**, 1637–1650 (1992)
10. Chevalier, M., Schlatter, P., Lundbladh, A., Henningson, S.D.: A pseudo spectral solver for incompressible boundary layer flows. Technical report Trita-Mek 7 (2007)
11. Fischer, P., Lottes, J., Kerkemeier, S.: nek5000 Web page (2008). http://nek5000.mcs.anl.gov
12. Goldstein, M.E., Leib, S.J., Cowley, S.J.: Distortion of a flat-plate boundary layer by free-stream vorticity normal to the plate. J. Fluid Mech. **237**, 231–260 (1992)
13. Goldstein, M.E., Wundrow, D.W.: On the Environmental Realizability of Algebraically Growing Disturbances and Their Relation to Klebanoff Modes. Theoret. Comput. Fluid Dyn. **10**, 171–186 (1998)
14. Haddad, O., Corke, T.: Boundary layer receptivity to free-stream sound on parabolic bodies. J. Fluid Mech. **368**(1), 1–26 (1998)
15. Levin, O., Henningson, D.S.: Exponential vs algebraic growth and transition prediction in boundary layer flow. Flow Turbul. Combust. **70**, 183–210 (2003)
16. Lin, N., Reed, H., Saric, W.: Effect of leading edge geometry on boundary-layer receptivity to freestream sound. In: Hussaini, M., Kumar, A., Streett, C. (eds.) Instability, Transition and Turbulence, Springer, Berlin (1992)
17. Luchini, P.: Reynolds-number-independent instability of the boundary layer over a flat surface: Optimal perturbations. J. Fluid Mech. **404**, 289–309 (2000)
18. Mao, X., Blackburn, H.M., Sherwin, S.J.: Optimal inflow boundary condition perturbations in steady stenotic flow. J. Fluid Mech. **705**, 306–321 (2012)
19. Mao, X., Blackburn, H.M., Sherwin, S.J.: Calculation of global optimal initial and boundary perturbations for the linearised incompressible navierstokes equations. J. Comput. Phys. **235**, 258–273 (2013)
20. Monokrousos, A., Åkervik, E., Brandt, L., Henningson, D.S.: Global three-dimensional optimal disturbances in the Blasius boundary-layer flow using time-steppers. J. Fluid Mech. **650**, 181–214 (2010)
21. Monokrousos, A., Bottaro, A., Brandt, L., Di Vita, A., Henningson, D.: Nonequilibrium thermodynamics and the optimal path to turbulence in shear flows. Phys. Rev. Lett. **106**(13), 134502 (2011)
22. Patera, A.T.: A spectral element method for fluid dynamics: Laminar flow in a channel expansion. J. Comput. Phys. **54**(3), 468–488 (1984)
23. Reddy, S.C., Henningson, D.S.: Energy growth in viscous channel flows. J. Fluid Mech. **252**, 209–238 (1993)
24. Saric, W.S., Reed, H.L., Kerschen, E.J.: Boundary-layer receptivity to freestream disturbances. Annu. Rev. Fluid Mech. **34**, 291–319 (2002)
25. Schrader, L.U., Brandt, L., Mavriplis, C., Henningson, D.S.: Receptivity to free-stream vorticity of flow past a flat plate with elliptic leading edge. J. Fluid Mech. **653**, 245–271 (2010)
26. Schrader, L.U., Brandt, L., Mavriplis, C., Henningson, D.S.: Nonlinear receptivity to oblique vortical modes in flow past an elliptic leading edge. J. Turbul. **13**, 1–16 (2012)
27. Tempelmann, D., Hanifi, A., Henningson, D.: Spatial optimal growth in three-dimensional boundary layers. J. Fluid Mech. **646**, 5–37 (2010)
28. Theofilis, V.: Global linear instability. Annu. Rev. Fluid Mech. **43**(1), 319–352 (2011)
29. Tuckerman, L.S., Barkley, D.: Bifurcation analysis for timesteppers. In: Doedel, E., Tuckerman, L.S. (eds.) IMA Volumes in Mathematics and its Applications. Numerical Methods for Bifurcation Problems and Large-Scale Dynamical Systems, vol. 119, pp. 543–566. Springer, New York (2000)
30. Tufo, H., Fischer, P.: Fast parallel direct solvers for coarse grid problems. Par. Dist. Comput. **61**(2), 151–177 (2001)

31. Wanderley, J.B.V., Corke, T.C.: Boundary layer receptivity to free-stream sound on elliptic leading edges of flat plates. J. Fluid Mech. **429**, 1–21 (2001)
32. Würz, W., Herr, S., Wörner, A., Rist, U., Wagner, S., Kachanov, Y.: Three-dimensional acoustic-roughness receptivity of a boundary layer on an airfoil: experiment and direct numerical simulations. J. Fluid Mech. **478**(1), 135–163 (2003)